Facile Synthesis of Mesoporous Silica SBA-15 with Additional Intra-Particle Porosities

Yu-Chuan Hsu, Ya-Ting Hsu, Hsi-Yen Hsu, and Chia-Min Yang*

Department of Chemistry, National Tsing Hua University, Hsinchu 300, Taiwan

Received September 11, 2006. Revised Manuscript Received December 6, 2006

Facile synthesis of mesoporous silica SBA-15 with additional intra-particle porosities has been demonstrated by using the carboxylate-terminated triblock copolymer Pluronic P123 as the structural directing agent. The thus prepared materials are promising for applications in which efficient diffusion of molecules is in great demand.

Introduction

Ordered mesoporous materials are attracting wide interest in fields of catalysis, selective sorbents for separation processes, regulated transport systems, and the immobilization of biomolecules.[1−6] Especially interesting for these applications are large-pore mesoporous silica materials prepared by using Pluronic-type triblock poly(ethylene oxide)−poly(propylene oxide)−poly(ethylene oxide) (EO_n-PO_mEO_n) copolymers as structural directing agents (SDAs).[7−14] A well-documented example is mesoporous silica SBA-15 synthesized by using Pluronic P123 ($EO_{20}PO_{70}EO_{20}$) as the SDA,[7−9] which has two-dimensional (2-D) hexagonal *p*6*mm* symmetry and channel-type mesopores. These materials generally have additional micropores in the silica walls resulting from the interpenetrating network of silica and hydrophilic EO chains formed during the synthesis.[15−18] The unique bimodal pore structure may bring great opportunities into advanced applications provided that methods of selective deposition of functional groups or guest species in either one or the other pore system are developed. Such a selective deposition may be achieved by applying the method of consecutive removal of the copolymer templates developed recently.[19−20]

On the other hand, practical applications of porous materials often require fast diffusion of molecules to and from the pore structure in which functional species are located. Since the diffusibility through confined nanochannels can be rather limited, efforts have been made to prepare MCM-41-type mesoporous materials with additional intra-particle and interconnected mesopores by, for instance, adding sodium chloride,[21] complexing polyalcohols,[22] or sodium tetrafluoroborate[23] or by postsynthesis treatments.[24,25] The need to create additional diffusion channels is even more crucial for mesoporous silica SBA-15 generally having a macroscopic morphology of rope-like, micrometer-sized aggregates.[7−9] However, there is still lack of synthetic methods to introduce additional intra-particle porosities in SBA-15 materials. Recently, the preparation of hierarchical macroporous−mesoporous silica monoliths has been reported.[26−29] These materials have 2-D hexagonal mesopore structure with long and straight channels parallel to the silica skeletons, just like that of SBA-15 materials, and between the silica skeletons are the interconnected macropores. In comparison to powdery SBA-15 materials, the macropores

* Corresponding author. Fax: 886-3-5165521. Tel.: 886-3-5731282. E-mail: cmyang@mx.nthu.edu.tw.

(1) Moller, K.; Bein, T. *Chem. Mater.* **1998**, *10*, 2950.
(2) Sayari, A.; Hamoudi, S. *Chem. Mater.* **2001**, *13*, 3151.
(3) Schüth, F.; Schmidt, W. *Adv. Mater.* **2002**, *14*, 629.
(4) Soler-Illia, G. J. de A. A.; Sanchez, C.; Lebeau, B.; Patarin, J. *Chem. Rev.* **2002**, *102*, 4093.
(5) Stein, A. *Adv. Mater.* **2003**, *15*, 763.
(6) Yiu, H. H. P.; Wright, P. A. *J. Mater. Chem.* **2005**, *15*, 3960.
(7) Zhao, D.; Feng, J.; Huo, Q.; Melosh, N.; Fredrickson, G. H.; Chmelka, B. F.; Stucky, G. D. *Science* **1998**, *279*, 548.
(8) Zhao, D.; Huo, Q.; Feng, J.; Chmelka, B. F.; Stucky, G. D. *J. Am. Chem. Soc.* **1998**, *120*, 6024.
(9) Choi, M.; Heo, W.; Kleitz, F.; Ryoo, R. *Chem. Commun.* **2003**, 1340.
(10) Kleitz, F.; Liu, D.; Anilkumar, G. M.; Park, I. -S.; Solovyov, L. A.; Shmakov, A. N.; Ryoo, R. *J. Phys. Chem. B* **2003**, *107*, 14296.
(11) Kleitz, F.; Solovyov, L. A.; Anilkumar, G. M.; Choi, S. H.; Ryoo, R. *Chem. Commun.* **2004**, 1536.
(12) Kim, T. W.; Ryoo, R.; Kruk, M.; Gierszal, K. P.; Jaroniec, M.; Kamiya, S.; Terasaki, O. *J. Phys. Chem. B* **2004**, *108*, 11480.
(13) Kleitz, F.; Choi, S. H.; Ryoo, R. *Chem. Commun.* **2003**, 2136.
(14) Kim, T. W.; Kleitz, F.; Paul, B.; Ryoo, R. *J. Am. Chem. Soc.* **2005**, *127*, 7601.
(15) Ryoo, R.; Ko, C. H.; Kruk, M.; Antochshuk, V.; Jaroniec, M. *J. Phys. Chem. B* **2000**, *104*, 11465.
(16) Impéror-Clerc, M.; Davidson, P.; Davidson, A. *J. Am. Chem. Soc.* **2000**, *122*, 11925.
(17) Ravikovitch, P. I.; Neimark, A. V. *J. Phys. Chem. B* **2001**, *105*, 6817.
(18) Galarneau, A.; Cambon, H.; Di Renzo, F.; Ryoo, R.; Choi, M.; Fajula, F. *New J. Chem.* **2003**, *27*, 73.
(19) Yang, C. M.; Zibrowius, B.; Schmidt, W.; Schüth, F. *Chem. Mater.* **2003**, *15*, 3739.
(20) Yang, C. M.; Zibrowius, B.; Schmidt, W.; Schüth, F. *Chem. Mater.* **2004**, *16*, 2918.
(21) Bagshaw, S. A. *Chem. Commun.* **1999**, 1785.
(22) Haskouri, J. E.; de Zárate, D. O.; Guillem, C.; Latorre, J.; Caldés, M.; Beltrán, A.; Beltrán, D.; Descalzo, A. B.; Rodríguez-López, G.; Martínez-Máñez, R.; Marcos, M. D.; Amorós, P. *Chem. Commun.* **2002**, 330.
(23) Okabe, A.; Niki, M.; Fukushima, T.; Aida, T. *J. Mater. Chem.* **2005**, *15*, 1329.
(24) Sun, J.; Shan, Z.; Maschmeyer, T.; Moulijn, J. A.; Coppens, M.-O. *Chem. Commun.* **2001**, 2670.
(25) Yuan, Z. Y.; Blin, J.-L.; Su, B. L. *Chem. Commun.* **2002**, 504.
(26) Hüsing, N.; Raab, C.; Torma, V.; Roig, A.; Peterlik, H. *Chem. Mater.* **2003**, *15*, 2690.
(27) Brandhuber, D.; Torma, V.; Raab, C.; Peterlik, H.; Kulak, A.; Hüsing, N. *Chem. Mater.* **2005**, *17*, 4262.
(28) Brandhuber, D.; Peterlik, H.; Hüsing, N. *J. Mater. Chem.* **2005**, *15*, 3896.
(29) Amatani, T.; Nakanishi, K.; Hirao, K.; Kodaira, T. *Chem. Mater.* **2005**, *17*, 2114.

10.1021/cm062167i CCC: $37.00
Published on Web 02/13/2007

in the silica monoliths are more like "inter-particle" rather than "intra-particle" porosity.

In this paper, we report a simple and facile synthesis of mesoporous silica SBA-15 materials with additional intra-particle porosities by using the carboxylate-terminated triblock copolymer Pluronic P123 (abbreviated P123-COOH). Carboxylic acids (e.g., formic acid, acetic acid, citric acid, or oxalic acid) are among popular acid catalysts for the hydrolysis and condensation of tetraalkoxysilane precursors.[30−33] When the P123-COOH copolymers form micellar structures in solution, the interfacial monolayer of carboxylate groups may facilitate the hydrolytic condensation of alkoxysilanes during the self-assembly process. In this study, we compare the SBA-15 materials synthesized with original hydroxyl-terminated P123 (abbreviated P123-OH) or P123-COOH in high (1.6 M) or low acid (0.3 M) conditions. We find that by using P123-COOH, the formation of hexagonally ordered SBA-15 materials is accelerated. Furthermore, the resulting materials have additional intra-particle meso- or macroporosities, depending on the acid concentration in the synthesis mixtures. The thus prepared SBA-15 materials have multi-modal and interconnected pore structures and are promising for practical applications in which good molecular diffusibility is one of the major concerns.

Experimental Section

Synthesis. The syntheses of mesoporous silica SBA-15 materials were performed in the high (1.6 M) or low (0.3 M) acid conditions,[8,9] and the triblock copolymers P123-OH and P123-COOH were used as SDAs. A typical synthesis started from the preparation of a hydrochloric acid (HCl) solution of the copolymer SDA. P123-COOH was produced in situ by adding stoichiometric amount of potassium dichromate ($K_2Cr_2O_7$) or potassium permanganate ($KMnO_4$) and additional HCl into the copolymer solution. The solution was stirred for hours until the reaction was complete. Tetraethoxysilane (TEOS) was then added into the copolymer solution, and the mixture was stirred at 35 °C for 20 h. The molar compositions were 1:5.9:193:0.017 TEOS/HCl/H_2O/P123 and 1:0.54:100:0.017 TEOS/HCl/H_2O/P123 for the syntheses in the high or low acid conditions, respectively. After aging at 90 °C for 1 day, the product was filtered, washed with acetone, and dried at 90 °C. The resulting samples are referred to as SBA-15-X-Y, where X denotes the acid condition of the synthesis mixture (X = H or L for the synthesis at 1.6 M or 0.3 M HCl, respectively) and Y denotes the type of end groups of the copolymer SDAs (Y = H or C for hydroxyl or carboxylate end groups, respectively). For instance, SBA-15-H-C refers to a SBA-15 material synthesized at the 1.6 M HCl using P123-COOH as the SDA. To remove the copolymers, the samples were calcined at 540 °C in air for 6 h.

Characterization. Powder X-ray diffraction (PXRD) data were obtained on a Mac Science 18MPX diffractometer using Cu Kα radiation. The in situ small-angle X-ray scattering/X-ray diffraction (SAXS/XRD) measurements were performed by using synchrotron X-ray (photon energy of 10.0 keV) on the beamline 17B3 at the National Synchrotron Radiation Research Center (NSRRC), Taiwan. Each reaction for the in situ measurement was carried out in a batch reactor, and the reaction mixture was continuously pumped through a Kapton sealed thin container, through which the X-ray beam passed and then back to the reactor at a pumping rate of 40 mL/min. Both the reactor and the container were thermostated to a desired temperature of 35 °C.

Nitrogen sorption isotherms were measured at 77 K using a Quantachrome Autosorb-1MP instrument. Each sample was evacuated at 200 °C for 12 h before measurement. The isotherms were analyzed by nonlocal density functional theory (NLDFT) method to evaluate surface area and pore size of the samples, and the kernel of NLDFT equilibrium capillary condensation isotherms of nitrogen at 77 K on silica was selected for the model isotherms (using adsorption branch and assuming cylindrical pore geometry). The total pore volumes were evaluated at a relative pressure of 0.95. Mercury porosimetry measurements were performed on a Micromeritics AutoPore III mercury porosimeter. The scanning electron microscopy (SEM) images were obtained on a JEOL JSM-6330F microscope, and the transmission electron microscopy (TEM) images were taken from ultramicrotomed samples using a JEOL JEM-2010 electron microscope. Elemental analysis was obtained by inductively coupled plasma atomic emission spectroscopy (ICP-AES) using a Jarrell-Ash-ICAP 9000 device. Solid-state ^{29}Si magic angle spinning (MAS) NMR spectra were measured on a Bruker DSX400WB spectrometer using a 7-mm MAS probe. UV−visible spectra were measured on a JASCO V-570 spectrophotometer.

Results and Discussion

The end-group oxidation of P123-OH to produce P123-COOH was complete in hours, and the reaction was monitored by tracing the amount of the remaining oxidant ($K_2Cr_2O_7$ or $KMnO_4$) using UV−visible spectroscopy. The yield of P123-COOH was estimated to be above 98% by acid−base titration. The possibility of P123-OH being dramatically modified or degraded during the end-group oxidation can be excluded, because the weight percentages of the copolymer SDA in the as-synthesized materials using P123-OH or P123-COOH were almost identical, and no structural change or transformation that might be related to such a possibility was observed on the materials synthesized with P123-COOH.

The influence of the end-group oxidation of the copolymer SDA is first reflected on the formation kinetics of the resulting SBA-15 materials. Figure 1 shows the in situ SAXS/XRD data of the samples synthesized in high acid condition. For SBA-15-H-H, one relatively sharp reflection and two less intense reflections appear suddenly after a reaction time of 47 min, and they can be indexed as the (100), (110), and (210) reflections of a 2-D hexagonal mesophase. The intensity of the (100) reflection continues to increase with time, which reflects an increase in the amount of ordered matter.[34] The *d*-spacing corresponding to the (100) reflection is 12.2 nm, and the value gradually decreases with time and reaches a stable minimum of 11.5 nm at 100 min. It suggests

(30) Charbouillot, Y.; Ravaine, D.; Armand, M.; Poinsignon, C. *J. Non-Cryst. Solids* **1988**, *103*, 325.
(31) Brinker, C. J.; Scherer, G. W. *Sol-Gel Science: The Physics and Chemistry of Sol-Gel Processing*; Academic Press: San Diego, CA, 1990.
(32) Auner, N., Weis, J., Eds. *Organosilicon Chemistry II: From Molecules to Materials*; VCH: New York, 1996.
(33) Green, W. H.; Le, K. P.; Grey, J.; Au, T. T.; Sailor, M. J. *Science* **1997**, *276*, 1826.
(34) Flodström, K.; Teixeira, C. V.; Amenitsch, H.; Alfredsson, V.; Lindén, M. *Langmuir* **2004**, *20*, 4885.

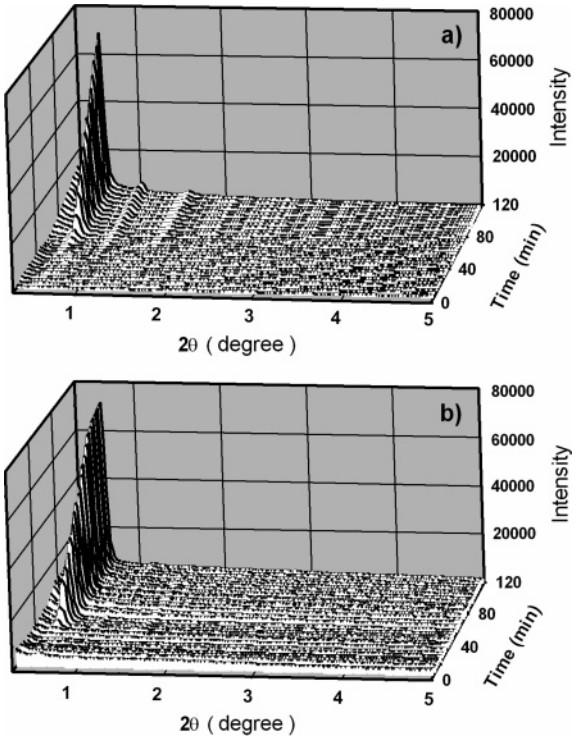

Figure 1. Time-resolved SAXS/XRD patterns of SBA-15-H-H (a) and SBA-15-H-C (b).

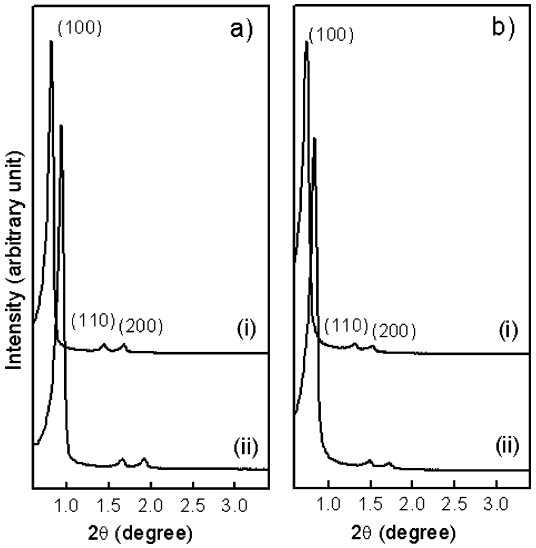

Figure 2. PXRD patterns of as-synthesized (i) and calcined (ii) materials of SBA-15-H-H (a) and SBA-15-H-C (b).

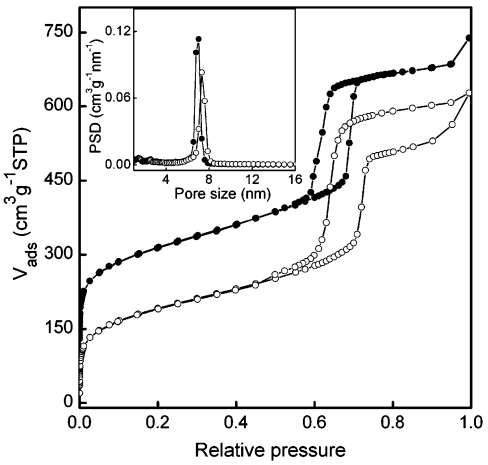

Figure 3. Nitrogen physisorption isotherms and the corresponding pore size distributions of calcined SBA-15-H-H (filled circles) and SBA-15-H-C (open circles). The isotherm of SBA-15-H-H is shifted by 100 cm^3 g^{-1} STP.

that the mesophase continues to contract during that period of reaction time. The observed structural evolution is in line with the previous study by Flodström et al.[34] In the synthesis of SBA-15-H-C, the (100) reflection already appears after a reaction time of 20 min, and its intensity increases rapidly with time. The shorter induction time for the (100) reflection of SBA-15-H-C than that of SBA-15-H-H suggests that the carboxylate end groups on the micelles of P123-COOH accelerate the formation of ordered mesostructures. The *d*-spacing calculated from the (100) reflection of SBA-15-H-C is also 12.2 nm, and it decreases to reach a stable minimum of 11.9 nm at 82 min. On the other hand, the (110) and (210) reflections of SBA-15-H-C first appear after a reaction time of 30 min, but the intensity of these two reflections remain low even after a reaction time of 120 min. Distinct from that for SBA-15-H-H or what has been observed previously,[34] the low intensity of the (100) and (210) reflections might be attributed to subtle difference of the degree of silica condensation in the P123-silica hybrid mesostructures.[34−36]

The structural properties of the samples after further aging at 90 °C for 1 day were then studied. Figure 2 compares the PXRD patterns of SBA-15-H-H and SBA-15-H-C before and after calcination at 540 °C. The pattern of SBA-15-H-C, just as that of SBA-15-H-H, exhibits (100), (110), and (200) reflections attributed to a hexagonal *p*6*mm* structure. This suggests that the end-group oxidation of P123 does not affect the formation of ordered mesoscopic structure. However, the cell parameter *a* for SBA-15-H-C is 13.8 nm, which is significantly larger than the value of 12.4 nm for SBA-15-H-H. After calcination, both samples undergo shrinkage, and the cell parameters become 12.3 and 10.8 nm for SBA-15-H-C and SBA-15-H-H, respectively. The calcined samples were further characterized by nitrogen physisorption measurement. The sorption isotherms of both samples, as shown in Figure 3, exhibit sharp steps with H1-type hysteresis loops corresponding to the filling of uniform mesopores with open cylindrical geometry.[37] The isotherms are analyzed by the NLDFT method, and Table 1 summarizes the structural properties of the materials. While both samples have similar surface areas, total pore volumes, and micropore volumes, SBA-15-H-C has a slightly larger pore diameter of 7.3 nm and significantly thicker pore wall of 5.0 nm than SBA-15-H-H with a pore diameter of 7.0 nm and pore wall thickness of 3.8 nm.

It is noteworthy that the H1 hysteresis loop in the isotherm of SBA-15-H-C does not close at the high relative pressure

(35) Sauer, J.; Marlow, F.; Schüth, F. *Phys. Chem. Chem. Phys.* **2001**, *3*, 5579.
(36) Zholobenko, V. L.; Khodakov, A. Y.; Durand, D. *Microporous Mesoporous Mater.* **2003**, *66*, 297.
(37) Sing, K. S. W.; Everett, D. H.; Haul, R. A. W.; Moscou, L.; Pierotti, R. A.; Rouquerol, J.; Siemieniewska, T. *Pure Appl. Chem.* **1985**, *57*, 603.

Table 1. Structural Properties of the Mesoporous Silica SBA-15 Materials

samples	unit cell *a* [nm]	pore diameter[a] [nm]	surface area[a] [$m^2\ g^{-1}$]	total pore volume[b] [$cm^3\ g^{-1}$]	micropore volume[a] [$cm^3\ g^{-1}$]	wall thickness [nm]
SBA-15-H-H	10.8 (12.4)[c]	7.0	707.8	0.94	0.06	3.8
SBA-15-H-C	12.3 (13.8)	7.3	655.5	0.92	0.06	5.0
SBA-15-L-H	11.2 (12.4)	6.8	757.8	1.10	0.05	4.4
SBA-15-L-C	11.2 (13.1)	7.0	488.6	0.72	0.03	4.2

[a] Calculated by the NLDFT method with the model of N_2 at 77 K on silica for cylindrical pores (using the adsorption branch). [b] Calculated at $P/P_0 = 0.95$. [c] In parentheses are the values for the as-synthesized materials.

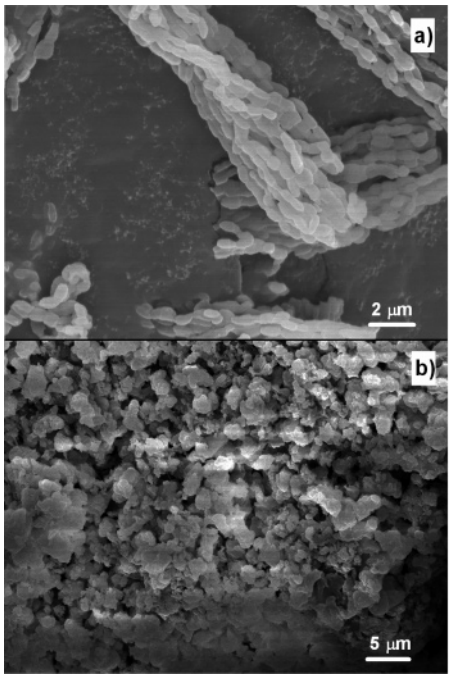

Figure 4. SEM images of (a) SBA-15-H-H and (b) SBA-15-H-C.

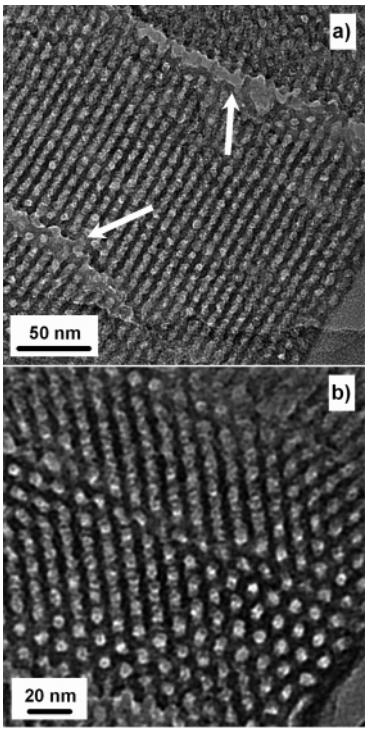

Figure 5. TEM images of ultramicrotomed SBA-15-H-C viewed normal to (a) or along the axis of the hexagonal pores (b). The arrows indicate the slit-type cracks in the sample.

region, like forming an additional H4-like hysteresis loop. Type H4 loops are often associated with narrow slit-type pores[37] that are either located inside a material or originated from inter-particle (textural) porosity. Therefore, SEM and TEM were further applied to investigate the morphology and the interior of the samples. The SEM images in Figure 4 show that while SBA-15-H-H consists of uniform and rope-like domains, just like other SBA-15-silica materials,[7−9] SBA-15-H-C is composed of aggregates of particles that are irregular in shape. Such a morphological difference of the two samples may be related to the end-group oxidation of the copolymer SDA. However, since the particles in SBA-15-H-C are several micrometers in size, the inter-particle porosity might not influence the physisorption isotherm of the sample. On the other hand, the TEM images of the ultramicrotomed SBA-15-H-C, as indicated in Figure 5a, reveal the presence of cracks well distributed in SBA-15-H-C. The cracks are 5−15 nm in width and several tens of nanometers in length, but they do not extend through the sample. It should be mentioned that the phenomenon is not an artifact arising from the ultramicrotoming, from which ordered striped patterns through the specimen are usually observed.[38] Considering the shape and dimension, these "slit-type" intra-particle cracks are likely to associate with the H4-like hysteresis loop in the sorption isotherm of SBA-15-H-C. The TEM images also show that the thickness of the pore walls in SBA-15-H-C is not very uniform, and one can find some breakages of the walls (Figure 5a) and cross sections of the mesopores that are not spherical in shape (Figure 5b). These structural features are seldom observed in typical SBA-15 materials.[7−9]

The carboxylate end-groups also affect the formation kinetics and the structural properties of the SBA-15 materials synthesized in the low acid condition. The induction times, during which the suspension of the synthesis solution was still translucent, for SBA-15-L-H and SBA-15-L-C were found to be about 35 and 60 min, respectively. It again suggests that the carboxylate groups on the micelles of P123-COOH accelerate the formation of the materials. After aging at 90 °C, the structural ordering of the resulting materials was studied by PXRD. Figure 6 shows the PXRD patterns of SBA-15-L-H and SBA-15-L-C before and after calcination. The PXRD pattern of SBA-15-L-C, just as that of SBA-15-L-H, exhibits (100), (110), and (200) reflections attributed to a hexagonal *p6mm* structure. The values of cell parameter *a* for SBA-15-L-C and SBA-15-L-H are 13.1 and 12.4 nm, respectively. After calcination, however, both materials have an identical cell parameter of 11.2 nm. This indicates that while the as-synthesized SBA-15-L-C has larger mesoscopic periodicity, it also undergoes more shrinkage during calcination than SBA-15-L-H does. Nitrogen

(38) Yuan, Z. Y.; Su, B. L. *Stud. Surf. Sci. Catal.* **2004**, *154*, 1525.

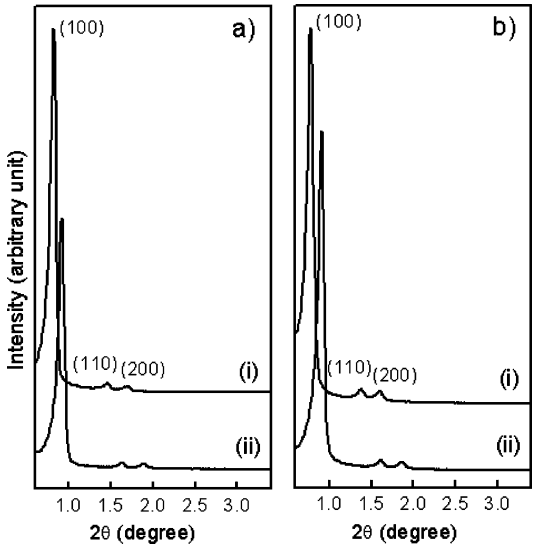

Figure 6. PXRD patterns of as-synthesized (i) and calcined (ii) materials of SBA-15-L-H (a) and SBA-15-L-C (b).

physisorption was also carried out for the calcined materials, and the resulting sorption isotherms are shown in Figure 7a. Both isotherms exhibit sharp steps with hysteresis loops corresponding to the filling of uniform mesopores with open cylindrical geometry. The pore size distributions for SBA-15-L-H and SBA-15-L-C are narrow, and the pore diameters are 6.8 and 7.0 nm, respectively. Combining with the results from PXRD, it suggests that SBA-15-L-C has slightly thinner pore walls of 4.2 nm than SBA-15-L-H with a wall thickness of 4.4 nm. On the other hand, as shown in Table 1, SBA-15-L-C has smaller total pore volume, surface area, and micropore volume than those of SBA-15-L-H.

The oxidation of the copolymer SDA even brings about greater changes in the macroscopic length scale for the material synthesized in low acid condition, and mercury porosimetery was applied to evaluate the macroporosity of the samples. It should be mentioned that nitrogen physisorption analysis is, in principle, capable of analyzing porous materials with pore diameter up to about 95 nm. However, for pores with less defined pore geometry and with pore diameter wider than tens of nanometers, the pore filling of physisorbed nitrogen happens in a relatively narrow range at relative pressure very close to unity and the pore size analysis may not be accurate. Complementary to nitrogen physisorption, mercury porosimetery is widely used to analyze porous structures with pore diameters ranging from tens of nanometers to micrometers. Figure 7b shows the cumulative mercury intrusion plots and the corresponding pore size distributions of the calcined materials. The cumulative pore volume of SBA-15-L-H stays nearly constant until the pore diameter reaches and exceeds the value of 5.5 μm. On the contrary, SBA-15-L-C exhibits a bimodal macropore structure with pore diameters of around 70 nm and 2.8 μm. The measured macropores of SBA-15-L-H and the large (2.8 μm) macropores in SBA-15-L-C are believed to be attributed to the inter-particle porosities of the materials. This is in line with the observation of SEM images shown in Figure 8, in which both SBA-15-L-H and SBA-15-L-C similarly consist of aggregates of rope-like domains with

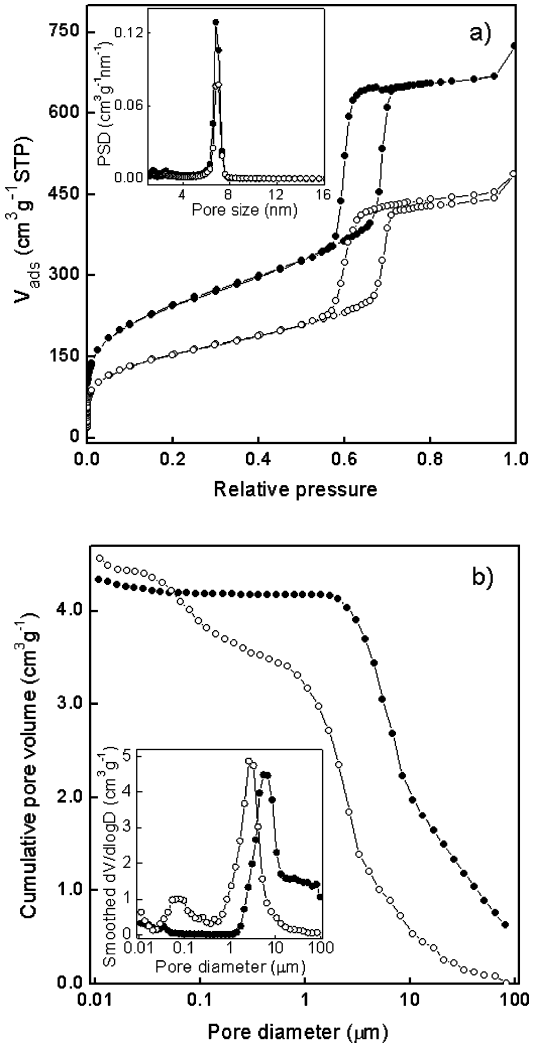

Figure 7. (a) Nitrogen physisorption isotherms and the corresponding pore size distributions of calcined SBA-15-L-H (filled circles) and SBA-15-L-C (open circles). (b) Cumulative mercury intrusion plots and the corresponding pore size distributions of calcined SBA-15-L-H (filled circles) and SBA-15-L-C (open circles).

sizes of 1−3 μm. On the other hand, the existence of the small (70 nm) macropores in SBA-15-L-C is unique for this type of large-pore mesoporous silica. Even though the pore size distribution is not very narrow, it contributes to a significant amount of the pore volume, around 0.5 cm^3 g^{-1}, in the material. Combining the contributions from the 7 nm mesopores and 70 nm macropores, the total volume of intra-particle porosity in SBA-15-L-C is estimated to be 1.2 cm^3 g^{-1}. The intra-particle macropores can be directly observed by TEM. In Figure 9, the TEM images of the ultramicrotomed SBA-15-L-C clearly show these macropores uniformly distributed inside the material. They are relatively irregular in shape, and their pore diameters are in the range of 50−150 nm. The observation is in accordance with the results of mercury porosimetry measurements. To our best knowledge, this type of porosity has never been observed in SBA-15-type materials.

The change of the morphology of SBA-15-H-C, the structural modulation, and the existence of uniformly distributed intra-particle porosities in SBA-15-H-C and SBA-15-L-C are obviously related to the end-group oxidation of

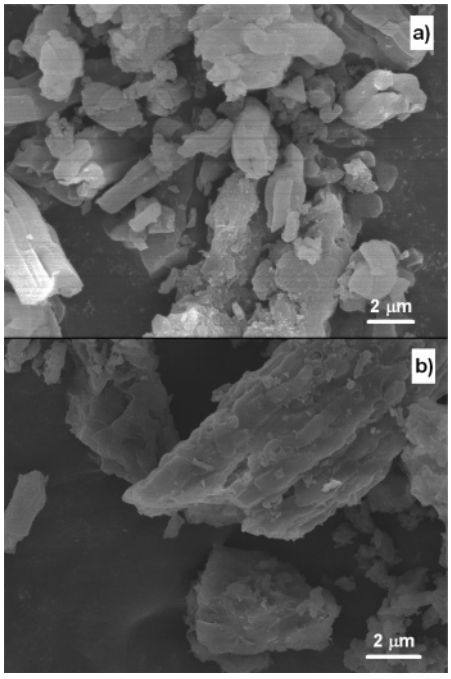

Figure 8. SEM images of (a) SBA-15-L-H and (b) SBA-15-L-C.

P123-OH. The end-group oxidation produces the carboxylate-terminated P123-COOH and the reduced oxidant, that is, the metal ions Cr^{3+} or Mn^{2+}. The concentration of the metal ions is very low, about 10 mM, and it is not considered to have appreciable influence on the structure or morphology of the resulting materials. Indeed, the control syntheses with 10 mM of $CrCl_3$ or $MnCl_2$ in the synthesis solution of P123-OH produced materials with nearly identical structural properties to those for SBA-15-H-H or SBA-15-L-H and without intra-particle porosities. On the other hand, the carboxylate end-groups of P123-COOH may serve as the on-site catalyst for the hydrolytic condensation of alkoxysilanes to produce P123-silica hybrid micelles[34] with a higher degree of silica condensation at the early stage of the synthesis. In conjunction with the kinetic studies by in situ SAXS/XRD, supportive evidence comes from ^{29}Si MAS NMR investigations. Since the degree of silica condensation can be significantly enhanced by the aging process, the as-synthesized SBA-15 materials before being aged at 90 °C, instead of aged samples, were collected for the study. Figure 10 shows the measured ^{29}Si MAS NMR spectra, and the intensity ratios of the Q^2, Q^3, and Q^4 lines (Q^n: $Si(OSi)_n(OH)_{4-n}$) are also calculated and shown. By comparing the two samples synthesized with the same acid concentration, one can find that the sample with P123-COOH as the SDA has the Q^4 line more intense than that for the other prepared with P123-OH. Such a difference in the relative intensity of the Q^4 line is larger for the materials synthesized in low acid condition. The results suggest that in addition to the acid catalyst HCl in the synthesis solution, the carboxylate end-groups on the micelles of P123-COOH may also catalyze the interfacial hydrolytic condensation of alkoxysilanes and affect the overall formation kinetics, which may probably in turn modulate the structure and the morphology of the resulting materials before or during the aging process.

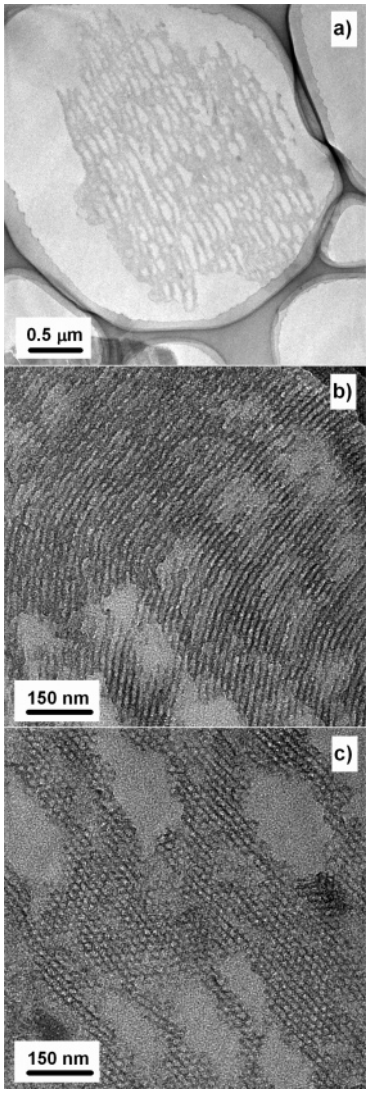

Figure 9. Low-magnification TEM image of ultramicrotomed SBA-15-L-C (a) and the TEM images of the sample viewed normal to (b) or along the axis of the hexagonal pores (c).

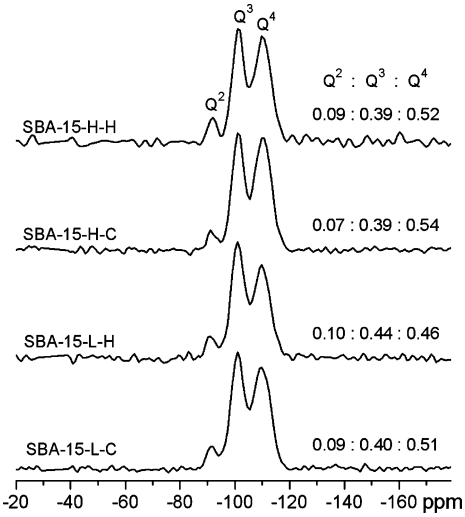

Figure 10. ^{29}Si MAS NMR spectra of the as-synthesized materials before aging at 90 °C. The intensity ratios are also calculated and shown.

Conclusions

We have demonstrated the facile synthesis of large-pore mesoporous silica SBA-15 materials with additional intra-particle porosities by using the carboxylate-terminated triblock copolymer P123 as the SDA. While the slit-type cracks have been found in the material synthesized in high acid condition, the intra-particle macropores have been observed in the material prepared with low acid concentration. The thus prepared SBA-15 materials have ordered pore structures with better connectivity, and they are promising for practical applications in which good molecular diffusibility is one of the major concerns.

Acknowledgment. The authors thank Lin Tsui for the mercury porosimetry measurements. National Science Council of the Republic of China is gratefully acknowledged for financial support under Contract No. NSC 93-2119-M-007-004.

Supporting Information Available: PXRD patterns of the as-synthesized samples (PDF). This material is available free of charge via the Internet at http://pubs.acs.org.

CM062167I